# Phosphorylation of human TRM9L integrates multiple stress-signaling pathways for tumor growth suppression

Chen Gu[1], Jillian Ramos[2], Ulrike Begley[3], Peter C. Dedon[1,4]*, Dragony Fu[2]*, Thomas J. Begley[3]*

**One Sentence Summary:** Phosphorylation drives TRM9L's tumor suppression activity.

**Affiliations:**

[1]Department of Biological Engineering, Massachusetts Institute of Technology, Cambridge, MA 02139.

[2]Department of Biology, Center for RNA Biology, University of Rochester, Rochester, New York 14627.

[3]The RNA Institute, University at Albany, SUNY, Albany, NY 12222.

[4]Singapore-MIT Alliance for Research and Technology, Singapore 138602.

*To whom correspondence should be addressed: pcdedon@mit.edu; dragonyfu@rochester.edu; tbegley@albany.edu

**Abstract**

The human tRNA methyltransferase 9-like gene (TRM9L, also known as KIAA1456) encodes a negative regulator of tumor growth that is frequently silenced in many forms of cancer. While TRM9L can inhibit tumor cell growth in vivo, the molecular mechanisms underlying the tumor inhibition activity of TRM9L are unknown. Here, we show that oxidative stress induces the rapid and dose-dependent phosphorylation of TRM9L within an intrinsically-disordered domain that is necessary for tumor growth suppression. Multiple serine residues are hyperphosphorylated in

response to oxidative stress. Using a chemical genetic approach, we identified a key serine residue in TRM9L that undergoes hyperphosphorylation downstream of the oxidative stress-activated MEK-ERK-RSK signaling cascade. Moreover, we found that phosphorylated TRM9L interacts with the 14-3-3 family of proteins, providing a link between oxidative stress and downstream cellular events involved in cell cycle control and proliferation. Mutation of the serine residues required for TRM9L hyperphosphorylation and 14-3-3 binding abolished the tumor inhibition activity of TRM9L. Our results uncover TRM9L as a key downstream effector of the ERK signaling pathway and elucidate a phospho-signaling regulatory mechanism underlying the tumor inhibition activity of TRM9L.

**Introduction**

A tumor suppressor gene has long been suspected on the short arm of chromosome 8, given the high frequency for loss-of-heterozygosity within that region of many cancer genomes (*1-4*). One candidate for this tumor suppressor is the tRNA methyltransferase 9-like gene (*TRM9L*, also known as *KIAA1456*) located at chromosome position 8p22 (*5*). The *TRM9L* gene locus is prone to rearrangement or deletion in many types of cancer, with TRM9L expression being greatly reduced or silenced by epigenetic mechanisms in breast, bladder, colorectal, cervical and testicular carcinomas (*5-8*). In further support of a tumor suppressor role for TRM9L, clinical data indicate that TRM9L expression strongly predicts prognosis, with low expression significantly correlated with early relapse or progression in breast and ovarian cancers (Supplementary Fig. S1) (*6, 9, 10*).

We have previously shown that re-expression of TRM9L in colon cancer cells reduces their proliferative capacity and confers sensitivity to the tumor environment of hypoxia (*8*). In addition to colon cancer cells, expression of TRM9L can also inhibit the proliferation, invasion

and metastasis of lung and ovarian cancer cells (*11, 12*). In the case of colon and ovarian cancer cells, the decrease in cellular proliferation caused by TRM9L expression has been linked to increased activity of the LIN-9 tumor suppressor pathway along with decreased HIF1-alpha response to hypoxic stress (*8, 12*). Moreover, re-expression of TRM9L can substantially reduce tumor formation in vivo, consistent with a tumor suppressor function for TRM9L (*8*). However, the specific molecular mechanisms underlying the tumor inhibition activity of TRM9L are unclear.

Mammalian TRM9L along with its paralog, AlkB homolog 8 (ALKBH8), are predicted homologs of the *S. cerevisiae* tRNA methyltransferase 9 (Trm9) enzyme (Supplementary Fig. S2A). In *S. cerevisiae*, Trm9p converts the modified wobble uridine, 5-carboxymethyluridine ($cm^5U$), into 5-methoxycarbonylmethyluridine ($mcm^5U$) in a subset of tRNAs (*13*). Human ALKBH8 has also been shown to catalyze the generation of $mcm^5U$ at the wobble position of tRNA and can partially rescue the formation of $mcm^5U$ in *S. cerevisiae* cells lacking Trm9 (*8, 14, 15*). These results indicate that ALKBH8 is a functional Trm9 homolog. In contrast to ALKBH8 however, TRM9L is unable to rescue the formation of $mcm^5U$ in Trm9-deficient *S. cerevisiae* cells and no methyltransferase activity has yet been demonstrated for TRM9L in vitro (*8*). Thus, TRM9L could require additional cofactors for methyltransferase activity or have acquired functions different than canonical Trm9 enzymes.

Here, we demonstrate that TRM9L is a phosphoprotein with phosphorylation playing a key role in its tumor inhibition behavior. Stress-dependent phosphorylation at multiple serine residues was found to increase sensitivity to tumorigenic stresses, control protein-protein interactions and suppress tumor growth. In particular, hyperphosphorylation of at least one TRM9L serine residue was found to be mediated by the MEK-ERK-RSK signaling pathway. Our

results position TRM9L as a new signaling node linking oxidative stress with a tumor growth suppression phenotype.

**Results**

*TRM9L contains an intrinsically-disordered domain that undergoes dynamic phosphorylation*

Using multiple protein folding and prediction algorithms, we examined the protein sequence of TRM9L for features that could provide insight into its mechanism of tumor suppression. Intriguingly, TRM9L is predicted to contain an intrinsically-disordered region embedded within the methyltransferase domain that is distinct in homology from yeast Trm9 and human ALKBH8 (Fig. 1A, Supplementary Figs. S2A, S2B)(*16*). Further *in silico* analysis revealed the presence of >30 predicted kinase phosphorylation motifs located within the disordered domain of TRM9L, with only one phosphorylation motif lying outside this domain (Supplementary Figs. S2C, S2D)(*17*). These predictions suggest that TRM9L could play a signaling role in tumor suppression as a phosphoprotein (*18, 19*).

Previous studies have shown that phospho-signaling pathways involved in tumor suppression are readily activated by loss of anchorage due to cell detachment (*20-25*). Thus, we investigated whether the phosphorylation status of TRM9L in human HCT116+TRM9L colon carcinoma cells was altered by trypsin-induced cell detachment, a standard tissue culture procedure. A rapid mechanical collection method that minimizes signaling changes was used as the control. The HCT116+TRM9L cell line was constructed by stably transducing the parental HCT116 colorectal carcinoma cell line, in which native *TRM9L* expression is undetectable (*8*), with a retroviral vector carrying FLAG-tagged *TRM9L*. For the mechanical collection method, cells were chilled on ice prior to scraping. The chilling step was presumed to slow down the activities of intracellular kinases and phosphatases and to help with preservation of basal

TRM9L phosphorylation status. To monitor the phosphorylation status of TRM9L, we used a gel mobility shift assay based upon the differential electrophoretic migration of phosphorylated proteins during SDS-PAGE after treatment with calf intestinal phosphatase (CIP) (*26*). From cells prepared by direct mechanical detachment, no major difference in TRM9L mobility was detected in lysates treated with CIP relative to untreated lysates (Fig. 1B "Scraping"). In contrast, from cells detached by trypsinization, CIP treatment of lysates led to an increase in TRM9L mobility (Fig. 1B "Trypsin"), which is consistent with phosphorylation of TRM9L. As additional evidence for phosphorylation, we carried out two-dimensional (2D) isoelectric focusing/SDS-PAGE to resolve the phosphorylated isoforms of TRM9L based upon their isoelectric point (pI), using lysate from cells treated with trypsinization. Using this approach, we also detected the CIP-induced disappearance of multiple low-pI TRM9L isoforms and the appearance of high-pI isoforms, again consistent with removal of phosphates from TRM9L (Fig. 1C). Thus, TRM9L is a phosphoprotein that undergoes inducible phosphorylation to generate multiple phosphorylated isoforms.

To validate and identify the phosphorylated residues, we mapped TRM9L phosphorylation sites by mass spectrometry-based phosphoproteomics. From lysate of HCT116+TRM9L cells harvested through trypsinization, TRM9L protein was enriched by anti-FLAG immunoprecipitation and hydrolyzed into peptides by trypsin. Phosphorylated peptides were further enriched by immobilized metal affinity chromatography and analyzed by mass spectrometry. After manual validation of the MS/MS spectra, six sites of TRM9L phosphorylation were assigned with high confidence, all at serine residues in the disordered domain: $Ser^{214}$, $Ser^{255}$, $Ser^{279}$, $Ser^{291}$, $Ser^{306}$ and $Ser^{380}$ (Figs. 1D, 1E, Supplementary Fig. 3).

These results demonstrate that TRM9L undergoes phosphorylation on multiple serine residues and suggests a potential role for phosphorylation in the biological function of TRM9L.

*Oxidative stress induces the hyperphosphorylation of TRM9L at Ser$^{380}$*

Besides loss of anchorage-dependent growth, oxidative stress constitutes another feature of cancer. Indeed, many tumor cells are characterized by elevated levels of reactive oxygen species (ROS) due to the Warburg effect and hypoxia-induced disruption of mitochondrial electron transport (*27, 28*). Based upon the critical role of oxidative stress management in tumor growth and metastasis (*29, 30*), we examined whether oxidative stress could also trigger the phosphorylation of TRM9L.

Using hydrogen peroxide ($H_2O_2$) as a model for oxidative stress, we observed a $H_2O_2$-induced shift in TRM9L migration to a lower mobility form in SDS-PAGE, indicative of TRM9L hyperphosphorylation (Figure 2A). The hyperphosphorylated form of TRM9L was rapid (<5 minutes post- $H_2O_2$), increased in an $H_2O_2$ dose-dependent manner and was detectable at $H_2O_2$ concentrations below the $LD_{50}$ of ~700 μM (Fig. 2B). Further 2D gel analysis revealed multiple $H_2O_2$-dependent phosphorylation states of TRM9L that could be abrogated by CIP treatment (Fig. 2C). Moreover, we found that exposure to menadione, a superoxide generator (*31*), could also increase the cellular phosphorylation of TRM9L (Figure 2D Top). In contrast, treatment with γ-radiation had no detectable effect on TRM9L phosphorylation (Figure 2D Bottom). Quantitative phosphoproteomics analysis revealed that HCT116+TRM9L cells treated with $H_2O_2$ increased phosphorylation at Ser$^{255}$ and Ser$^{291}$ in TRM9L with no significant change

in $Ser^{214}$ phosphorylation (Fig. 2E). Phosphorylation at other serine residues could not be confidently quantified due to limitations of the phosphoproteomics method.

To determine which phosphorylation sites contributed to the TRM9L mobility shift observed by SDS-PAGE, we generated serine-to-alanine mutants of TRM9L at residues 214, 255, 291 and 380. We found that mutation of serine 380 abolished the TRM9L gel mobility shift induced by $H_2O_2$, with no such effect detected for the other mutants (Fig. 2F). Further analysis of purified TRM9L-S380A mutant protein from $H_2O_2$-treated cells via mass spectrometry revealed that phosphorylation of $Ser^{214}$, $Ser^{255}$, $Ser^{291}$, and $Ser^{306}$ was still detected even though position 380 was unable to be phosphorylated (Supplementary Fig. 4). These results indicate that the $H_2O_2$-induced low-mobility form of TRM9L apparent by SDS-PAGE resulted from $H_2O_2$-induced phosphorylation of $Ser^{380}$. Thus, the relative mobility shift of TRM9L in SDS-PAGE reflects the degree of $Ser^{380}$ phosphorylation. Together, our results uncover an oxidative stress-induced phospho-signaling pathway that triggers the phosphorylation of multiple serines within TRM9L, including a major TRM9L isoform generated by hyperphosphorylation of $Ser^{380}$.

*Hyperphosphorylation of TRM9L $Ser^{380}$ is dependent upon activation of the ERK-RSK signaling pathway*

ROS leads to the activation of several intracellular signaling networks that are required for maintaining ROS homeostasis and cellular proliferation (*32, 33*). To decipher the signaling pathways that modulate phosphorylation of TRM9L, we used a chemical genetic approach based upon a panel of kinase inhibitors to look for molecules that could inhibit formation of the low-mobility hyperphosphorylated form of TRM9L in SDS-PAGE (Supplementary Table S1). We found that $H_2O_2$-induced hyperphosphorylation of TRM9L $Ser^{380}$ was diminished in cells pre-

treated with inhibitors of the Mitogen-activated protein kinase/Extracellular signal-regulated kinase Kinases, MEK1 and MEK2 (Table 1, U0126 and PD98059). Although commonly thought to be downstream of growth factors, Extracellular signal-Regulated Kinases (ERK) have been reported to be activated by oxidative stress; for instance, oxidative stress including $H_2O_2$ can activate membrane-associated receptor tyrosine kinases such as the Epidermal Growth Factor Receptor to initiate the ERK signaling cascade (Fig. 3A)(*34-36*). Indeed, we confirmed that $H_2O_2$ can induce the activation of the ERK signaling pathway in HCT116+TRM9L cells based upon $H_2O_2$-induced phosphorylation of ERK1/2 (P-ERK1/2) (Fig. 3B, +$H_2O_2$). Moreover, we validated that pre-incubation with the MEK1/2 inhibitor U0126 abolished the $H_2O_2$-induced phosphorylation of ERK1/2 and the hyperphosphorylation of TRM9L $Ser^{380}$ (Figure 3B, +$H_2O_2$ +U0126). In contrast to inhibitors of the ERK signaling pathway, no major effect on TRM9L hyperphosphorylation was detected for the other kinase inhibitors, including inhibitors of the related MAP kinases, p38 and JNK (Supplementary Table S1). These results support the idea that oxidative stress-induced hyperphosphorylation of TRM9L is primarily dependent upon activation of the MEK-ERK signaling pathway.

As a major transducer of the ERK signaling pathway, ribosomal protein S6 kinase (RSK) phosphorylates numerous downstream targets including those that activate the oxidative stress response (Fig. 3A) (*37, 38*). Among the TRM9L phosphorylation sites confirmed here, we found that $Ser^{380}$ lies within a consensus motif (RRIpS) for RSK phosphorylation (Fig. 1E) (*39*). To test the role of RSK in hyperphosphorylation of TRM9L $Ser^{380}$, we inhibited all four isoforms of RSK using the cell permeable inhibitor BI-D1870 and found that RSK inhibition can indeed decrease $H_2O_2$-induced hyperphosphorylation of TRM9L $Ser^{380}$ (Fig. 3C). A similar inhibition of $H_2O_2$-induced hyperphosphorylation of TRM9L $Ser^{380}$ was also observed for a different

compound, AZD7762, which was initially developed as a CHEK1/2 inhibitor but was later found to be a potent inhibitor of RSK2 and RSK3 as well (Fig. 3D) (*40*). Collectively, these findings reveal TRM9L as a phosphorylation target downstream of the MEK-ERK-RSK signaling pathway in response to oxidative stress.

*TRM9L interacts with 14-3-3 signaling proteins in a phosphorylation-dependent manner*

The $H_2O_2$-induced phosphorylation of TRM9L could promote protein-protein interactions with further downstream effectors to carry out the tumor inhibition role of TRM9L. To identify TRM9L-interacting proteins, we affinity-purified TRM9L from HEK293 cells detached by trypsin, followed by analysis of associated proteins. As a control study, we also purified ALKBH8, a paralog of TRM9L (*14*). Silver stain analysis of the eluted fractions revealed the presence of several bands at ~28 kDa specifically in the TRM9L pulldown but not with vector control or ALKBH8 (Fig. 4A). Mass spectrometric analysis of the gel-excised 28 kDa bands revealed the presence of the 14-3-3 family of signaling proteins (Fig. 4B). Since many portions of the primary sequence of each 14-3-3 protein are identical and cannot be distinguished by mass spectrometry, we validated the identity of specific 14-3-3 proteins using immunoblotting with antibodies specific to each 14-3-3 protein. Here we detected the specific co-purification of 14-3-3 gamma, epsilon and eta with TRM9L, while no signal was detected for the other 14-3-3 proteins in any of the purifications (Fig. 4C).

The 14-3-3 family of signaling proteins, via binding to target motifs containing phospho-serine or phospho-threonine, are well-known regulators of proteins phosphorylated by RSK (*41-43*). Moreover, 14-3-3 proteins form homo- or hetero-dimers that interact with phosphorylated serine/threonine residues of client proteins (*44*). Of note, the phosphorylated $Ser^{214}$ site of

TRM9L lies within a canonical 14-3-3 binding motif (RSHpSVG) while $Ser^{255}$ is a partial match for a consensus 14-3-3 binding motif (Fig. 1E) (*45*). Using the TRM9L serine to alanine mutants described above, we found that mutation of either $Ser^{214}$ or $Ser^{255}$ abrogated binding of all 14-3-3 proteins to TRM9L as detected by silver stain or immunoblotting (Fig. 4C). These results highlight an interaction between 14-3-3 proteins and TRM9L that is dependent upon phosphorylation of serine residues.

*TRM9L phosphorylation is required for oxidative stress hypersensitization and tumor suppression*

Given the critical roles played by 14-3-3 proteins (*45*) and MEK-ERK-RSK signaling (*46*) in modulating cell cycle progression and apoptosis in response to developmental and environmental cues, the results to this point suggest a key role for TRM9L phosphorylation in controlling cell fate in response to tumorigenic conditions. To test the cellular function of TRM9L phosphorylation, we quantified the effect of TRM9L on oxidative stress survival in two types of colorectal carcinoma cells with distinct origins, HCT116 and SW620. In both cell lines, expression of native *TRM9L* is undetectable (*8*). We found that re-expression of TRM9L in either human HCT116 or SW620 colon carcinoma cells leads to increased sensitivity to oxidative stress induced by $H_2O_2$ (Figs. 5A, 5C). In contrast, TRM9L expression had no effect on cellular sensitivity to ionizing radiation (Figs. 5B, 5D), consistent with the lack of TRM9L hyperphosphorylation induced by γ-radiation (Fig. 2D Bottom). In addition, treatment of HCT116+TRM9L cells with $H_2O_2$ in the presence of the RSK inhibitor AZD7762 resulted in increased survival compared to HCT116+TRM9L cells treated with $H_2O_2$ alone (Fig. 5E), whereas the AZD7762 pre-treatment did not cause any significant difference in the survival of

HCT116+LacZ cells treated with $H_2O_2$ (Fig. 5F). This suggested that the increase in the survival of HCT116+TRM9L cells mediated by AZD7762 was due to its effect on TRM9L protein and not due to other effects it might have on the cell. Thus, re-expression of TRM9L in colorectal cancer cells leads to oxidative stress-hypersensitization with TRM9L phosphorylation playing a key role in determining cell survival.

Finally, we tested whether the phosphorylation of TRM9L plays a role in tumor suppression using an in vivo xenograft model based upon the chicken chorioallantoic membrane (CAM) tumor formation assay (*47*). We tested the tumor-forming potential of SW620 colon cells expressing either LacZ, WT-TRM9L or the TRM9L mutants, S214A, S255A, S291A and S380A. The SW620 cell line was chosen for its ability to form a solid tumor in the CAM model (*48*). Confirming our previous results (*8*), re-expression of WT-TRM9L could greatly suppress SW620 tumor cell growth relative to control SW620 cells expressing LacZ alone (Fig. 5G). Strikingly, the TRM9L mutants S214A, S255A, and S380A were greatly impaired for tumor growth suppressor activity relative to WT-TRM9L (Fig. 5G). In contrast, mutation of $Ser^{291}$ had no effect on the tumor suppressor activity of TRM9L, consistent with the lack of a detectable function for that particular phosphorylated residue. Altogether, these findings unveil a pivotal role for TRM9L hyperphosphorylation in determining cancer cell survival and tumor growth suppression through the activation of a distinct MEK-ERK-RSK signaling pathway.

**Discussion**

Here, we show that TRM9L is phosphorylated at multiple serine residues and that certain types of oxidative stress induce the hyperphosphorylation of TRM9L. Furthermore, we provide evidence that the effect of TRM9L on cell proliferation is mediated by ROS-dependent phosphorylation linked to ERK-RSK signaling and 14-3-3 binding. Collectively, our studies

establish that the tumor growth suppressing activity of TRM9L is dependent upon on at least three of six phosphorylation sites linked to these pathways. These results support a model in which an ERK/RSK-dependent phospho-signaling regulatory mechanism underlies the tumor inhibiting behavior of TRM9L in response to oxidative stress (Fig. 6).

The activation of ERK by $H_2O_2$ cannot be overlooked given the central role of ERK as a proto-oncogene and the association of mutations in EGFR-Ras-Raf-MEK-ERK pathway components with tumorigenesis and metastasis (*49*), as well as the central role of ROS in tumorigenic inflammation (*50*) and the hypoxic tumor microenvironment (*27*). Previous studies have demonstrated $H_2O_2$ activation of ERK1 in hepatocytes, with functional distinctions between EGFR- and ROS-induced ERK activation (*38*). Studies in $H_2O_2$-treated glioma cells further revealed ERK-dependent RSK activation (*51*). While further work is needed to delineate the molecular mechanism, our studies provide a contextual link between ROS, the ERK-RSK pathway, TRM9L phosphorylation-dependent 14-3-3 binding, and tumor growth suppression. This is consistent with the observation that TRM9L expression promotes cellular senescence and sensitivity to hypoxia as well as ROS (*8*), with phospho-signaling now added as a modulator of TRM9L activity.

Another major consequence of TRM9L phosphorylation involves putative conformational changes controlling protein-protein interactions. The intrinsically disordered domain of TRM9L, which is absent in yeast Trm9 and human ALKBH8, is host to >30 kinase recognition and protein-binding motifs (Supplementary Fig S2C). Emerging evidence points to disordered domains as critical features of many signaling and regulatory proteins, with phosphorylation and protein-protein interactions stabilizing and organizing the domains for functional activity (*18, 19*). Of these 30 sites, we demonstrated functional activity for 3 serine

residues in RSK phosphorylation and 14-3-3 binding. Through mutagenesis studies, we found that 14-3-3 binding depends on phosphorylation of both $Ser^{214}$ positioned in a 14-3-3 binding motif and the $Ser^{255}$ site lying in a partial 14-3-3 consensus motif (Fig. 4C), with only $Ser^{255}$ phosphorylation increasing during oxidative stress (Fig. 2E). This raises the possibility that 14-3-3 binding to TRM9L increases during oxidative stress as part of the $H_2O_2$-activated ERK/RSK pathway. Considering that chaperone-like stabilization of binding partners is one of the many functions of 14-3-3 proteins (*45*), the binding of 14-3-3 proteins could further stabilize the intrinsically-disordered domain of TRM9L to facilitate an active conformation.

Finally, a surprising feature of TRM9L is its hyperphosphorylation induced by $H_2O_2$ but not by ionizing radiation, at least for $Ser^{380}$. The observation that TRM9L expression sensitizes cells to $H_2O_2$ exposure (Fig. 5A, 5C) is consistent our previous observation that TRM9L promotes senescence and increases hypoxia sensitivity to suppress tumor growth (*8*). However, the lack of an effect of TRM9L on ionizing radiation-induced cytotoxicity points to very different chemical mechanisms underlying $H_2O_2$ and ionizing radiation stress. Both agents can form hydroxyl radical (HO•), but this reaction requires a redox-active metal for $H_2O_2$, which localizes the damage to within 100 Å of the metal due to the high reactivity of HO• (*50*). On the other hand, the HO• and other radical species produced along the essentially random cellular tracks of photons during γ-radiation are not targeted (*52, 53*). Differences between $H_2O_2$ and ionizing radiation are also apparent at the level of transcriptional activation and repression in human cells (*54, 55*). Along with the well-established signaling function of $H_2O_2$ by virtue of selective oxidation of cysteines in signaling proteins (*56*), these differences may explain how the signaling pathways that lead to hyperphosphorylation of TRM9L, including the MEK-ERK-RSK pathway, differentiate between $H_2O_2$ and ionizing radiation in TRM9L's decision-making function to influence cell survival and

promote senescence. Future studies will be devoted to understanding this distinction at a molecular and atomic level.

## Materials and Methods

### *Primary sequence analysis*

The primary amino acid sequence corresponding to Uniprot # Q9P272-1 was used for all *in silico* analysis. Prediction of phosphorylation sites was made by entering the primary amino acid sequence into DISPHOS 1.3 (http://www.dabi.temple.edu/disphos/) with setting on "default predictor". For the same purpose, the PHOSIDA predictor for Phosphorylation in *Homo sapiens* (http://141.61.102.18/phosida/index.aspx, select "Tools" Tab) was also used. Prediction of protein folding intrinsic disorderedness was made by entering the primary amino acid sequence into FoldIndex (https://fold.weizmann.ac.il/fldbin/findex) with the following settings: window = 51, step = 1.

### *Reagents*

Unless otherwise stated, reagents were of ACS grade or better (Sigma-Aldrich). Antibodies included: anti-FLAG M2 and goat anti-mouse-HRP (Sigma-Aldrich, St. Louis, MO); anti-phospho-ERK1/2 ($Thr^{202}/Tyr^{204}$), anti-ERK1/2, anti-RSK2, anti-PARP1, and anti-14-3-3 Alpha/Beta, Gamma, Delta/Zeta, Eta, Tau 14-3-3 Family Antibody Sampler Kit (Cell Signaling Technology, Danvers, MA); monoclonal anti-Streptag II (Thermo Fisher); anti-TRMT112 (F-7), anti-14-3-3 Epsilon (T-16), and goat anti-Rabbit-HRP (Santa Cruz Biotech); anti-14-3-3 Sigma (Bethyl Laboratories); goat anti-rabbit 800 (Thermo Fisher); and goat anti-mouse 680 (Licor).

### *Cell line construction*

HCT116 and SW620 cells expressing LacZ or FLAG-tagged TRM9L were prepared as described previously (*8*). The FLAG-tagged TRM9L coding sequence contains three naturally occurring single-nucleotide polymorphisms (SNP) that differ from the SwissProt (www.uniprot.org) reference sequence: H150R, C207G, and G304E. Cell lines were maintained in DMEM (4.5 g/L glucose, glutamine-free, Lonza, Basel, Switzerland) supplemented with 10% FBS (Atlantic Biologicals, Flowery Branch, GA), 100 U/ml penicillin, 100 μg/ml streptomycin (Pen/strep, Lonza) and 2 mM glutamine (Lonza) in humidified 5% $CO_2$ at 37 °C. For TRM9L point mutants, site-directed mutagenesis was performed using PCR-based approaches and verified by DNA sequencing. DNA primers were designed to replace the appropriate bases in the coding sequence of TRM9L: serine (AGT) to alanine (GCC) at position 214 (S214A mutant); serine (TCT) to alanine (GCT) at position 255 (S255A mutant); serine (AGT) to alanine (GCT) at position 291 (S291A mutant); and serine (TGT) to alanine (GCA) at position 380 (S380A mutant). Stable SW620 and HCT116 cells expressing TRM9L mutant constructs were made by retroviral transduction as described previously (*8*). The 293T human embryonic kidney and derivative cell lines were cultured in Dulbecco's Minimal Essential Medium (DMEM) containing 10% fetal bovine serum (Thermo Fisher), 2 mM L-alanyl-L-glutamine (GlutaMax, Gibco) and 1% penicillin/streptomycin (Gibco).

*Treatment with oxidants*

Cells ($1x10^6$) were seeded in 6-well plates and covered with medium (2 ml). After overnight incubation at 37 °C, medium was aspirated, washed once with PBS (tissue-culture grade, Lonza), and covered with 2 ml of ambient-temperature FBS-free media, followed by addition of oxidants ($H_2O_2$ diluted in PBS, menadione diluted in DMSO, or PBS alone as a control). The plate was

immediately incubated at 37 °C. At various times, medium was aspirated and cells washed with PBS before proceeding to lysis.

*Kinase inhibitor treatments*

Cells ($1x10^6$) were seeded in 6-well plates and covered with medium (2 ml). After overnight incubation, kinase inhibitors diluted in DMSO were added: U0126 (10 μM), selective ERK1/2 inhibitor (Cell Signaling Technology); AZD7762 (150 nM), selective inhibitor of checkpoint kinases (Chk) 1 and Chk2, also inhibits RSK2/3 (Cayman Chemicals, Ann Arbor, MI); BI-D1870 (10 μM) potent inhibitor of the NTKD of RSK1-4 (Cayman Chemicals). Cells were incubated at 37 °C for an additional 75 min and then treated with oxidants as described above. Kinase inhibitors were also added in the FBS-free media used for $H_2O_2$ treatment.

*Survival measurement*

After cells were treated with oxidants as described above or irradiated with the desired dose of $^{137}Cs$ γ-radiation, they were washed with PBS once and replenished with fresh media. Cells were continuously incubated for 24 hrs before being trypsinized. The number of surviving cells was determined by resistance to Trypan Blue staining. For each cell line, the number of surviving cells in each treatment condition was compared against that in the untreated control sample to obtain the percentage survival. Statistical significance was determined by a Student T-test at each dose of treatment.

*Cell lysate preparation*

Unless otherwise stated, cells were detached from tissue culture plates by trypsinization (0.05% Trypsin-EDTA without $Ca^{2+}$/$Mg^{2+}$, Lonza) at 37 °C and collected by centrifugation (500xg, 5 min, 4 °C). After aspirating medium, the cell pellet was resuspended in lysis buffer consisting of

PBS, 1% Triton-X, 2 mM EDTA, 1:100 mammalian cell protease inhibitors (Sigma-Aldrich) and 1:100 phosphatase inhibitor (HALT, Thermo Fisher). Cells were lysed by incubation on ice for 20 min, followed by pipetting to further disrupt the cells. The lysate was cleared by centrifugation (5,000xg, 10 min, 4 °C).

For studies with $H_2O_2$ or menadione, cells were washed once with PBS after treatment, covered with PBS, and immediately placed on ice for 10 min. They were then mechanically dislodged from plates using a cell scraper and collected by centrifugation (500xg, 5 min, 4 °C). Whole cell lysates were prepared as described above.

*Dephosphorylation reactions*

Cell lysates (~100 μg total protein) prepared in the absence of phosphatase inhibitor were diluted with CIP reaction buffer consisting of 50 mM Tris, pH 7.9, 5 mM $MgCl_2$, 0.1 mM dithiothreitol (DTT), and 1:100 protease inhibitor (Sigma-Aldrich) to a total volume of 150 μl. CIP (15 μl, 150 units, New England Biolabs, Ipswich, MA) was then added and the reaction mixture was incubated at 30 °C for 15 min. The reaction was terminated by addition of Laemmli buffer (Bio-Rad Laboratories, Hercules, CA) for SDS-PAGE or by adding a 6X volume of ice-cold acetone for 2D gel analysis.

*One-dimensional SDS-PAGE Western blots*

Cell lysate was mixed with 4X Laemmli buffer (3:1) and heated at 95 °C for 5 min before loading onto a 1.5-mm-thick 8% acrylamide gel (bisacrylamide:acrylamide = 1:37.5, 375 mM Tris-HCl, pH = 8.8, 0.1% w/v SDS, 0.1% w/v ammonium persulfate [APS], 0.01% v/v tetramethylethylenediamine [TEMED]) with a 4% acrylamide stacking layer (bisacrylamide:acrylamide = 1:37.5, 125 mM Tris-HCl, pH = 6.8, 0.1% w/v SDS, 0.1% w/v

APS, 0.01% v/v TEMED) poured in Bio-Rad Mini-PROTEAN short plates and was left at ambient temperature overnight prior to use. After loading, the gel was run in a Bio-Rad Mini-PROTEAN III electrophoresis system at 150 V for 1 hr, followed by electro-transfer to PVDF membrane (0.2 μm pore, Bio-Rad Laboratories) using the standard tank transfer method at 300 mA for 1 hr. The PVDF membrane was then blocked with 3% milk at room temperature for 30 minutes, probed by the primary antibody at 4 °C overnight, secondary antibody at room temperature for 1 hr, and finally visualized using ECL (SuperSignal West Dura, Thermo Fisher) and a CCD camera (FluorChem 8900, Alpha Innotech, San Leandro, CA). The degree of phosphorylation was calculated as the ratio of the intensity of the slower band to that of the faster band. Each data point represents the mean ± standard deviation for three biological replicates. Samples were compared using an unpaired Student T-test ($p < 0.05$).

*Two-dimensional IEF-SDS-PAGE Western Blots*

Ice-cold acetone was added to cleared cell lysate (~100 μg total protein) at 6:1 v/v and the mixture was stored at -20 °C overnight to precipitate proteins. The suspension was centrifuged (16,000xg, 20 min, 4 °C) and the resulting pellet was washed with ice-cold 80% acetone and air-dried to remove acetone. The pellet was fully dissolved in 125 μl IPG dissolution buffer (7 M urea, 2 M thiourea, 1% w/v DTT, and 5% glycerol, 1% IPG solution, pH 4-7; GE Amersham, Chicago, IL), and the solution was loaded evenly onto a 70 mm IPG strip (pH 4-7, GE Amersham). IEF was performed on an Agilent 3100 Off-gel fractionator (Agilent Technologies, Santa Clara, CA) with the following settings: 8 kV•hr, max current = 50 μA, max voltage = 4500 V, 4 °C. After the desired run time was reached, the IPG strip was removed from the fractionator and soaked in 10 ml of equilibration buffer (6M urea, 2% w/v SDS, 50mM Tris-HCl, pH 8.8, 20% glycerol, 1% w/v DTT, bromophenol blue) for 10 min at ambient temperature. It

was then positioned atop a 1.5-mm 8% acrylamide gel and encased in molten agar (1% agarose in 1X Tris-glycine running buffer). Following agar solidification, the gel (2$^{nd}$ dimension) was run and the multiple isoforms of TRM9L were eventually visualized in Western blot, as described above.

*Mass spectrometry-based phosphoproteomics*

Studies were initiated by immunoprecipitation of TRM9L. Protein G magnetic beads (New England Biolabs) were covalently cross-linked to anti-FLAG M2 using the dimethyl pimelimidate (DMP) procedure (https://www.neb.com/protocols/1/01/01/cross-linking-of-igg-to-protein-a-or-g-beads). Whole-cell lysates from treated and untreated HCT116 cells stably expressing TRM9L were diluted with cold lysis buffer to a volume of 300 µl (~3 µg/µl protein). Antibody-linked protein G beads (15 µl) were added and the mixture shaken gently at 4 °C overnight. The next morning, the depleted lysate was aspirated and the magnetic beads were washed 4-times with 800 µl cold PBS. Antibody-bound proteins were eluted once with 40 µl and twice with 20 µl of 6 M urea at ambient temperature for 10 min.

Proteins in the 6M urea eluate were reduced (10 mM dithiothreitol, 56 °C, 45 min) and alkylated (50 mM iodoacetamide; ambient temperature, dark, 1 hr), and subsequently digested with 2.5 µg trypsin (sequencing grade, Promega, Madison, WI; ambient temperature overnight, 100 mM ammonium acetate, pH 8.9). Following trypsin quenching with formic acid (5%), peptides were desalted using C18 SpinTips (Protea, Morgantown, WV), lyophilized and stored at −80 °C.

Peptides were labeled with TMT 10plex (Thermo Fisher) by dissolving lyophilized samples in 70 µl ethanol and 30 µl of 500 mM triethylammonium bicarbonate, pH 8.5, and then adding TMT reagent in 30 µl of anhydrous acetonitrile. The solution was vortexed and incubated at

ambient temperature for 1 hr. Labeled samples were combined and concentrated in a vacuum centrifuge.

Phosphorylated peptides were enriched using a modification of a published Fe-NTA affinity purification protocol(*57*). Briefly, following nickel removal from Ni-NTA agarose (Qiagen, Venlo, Netherlands) with 100 mM EDTA, 100 mM $FeCl_3$ as added to generate Fe-NTA. Acidified peptides were then added and incubated for 1 hr at ambient temperature. Phosphopeptides were eluted with 250 mM sodium phosphate. The flow-through of total peptides were also collected.

For LC-MS/MS analysis, reversed-phase HPLC was performed using an in-house generated pre-column (6 cm) packed with C18 (10 µm particle size) and a self-packed 12 cm, 10 µm-tip analytical column (New Objective, Woburn, MA) packed with C18 (5 µm particle size), mounted in an EASY- nLC1000 (Thermo Fisher) and eluted with a 70-min gradient (200 nl/min) for enriched phosphopeptides and a 140-min gradient for flow-through total peptides. The eluent was directed into a nanoelectrospray ionization-mode QExactive Plus mass spectrometer (Thermo Fisher). The mass spectrometer was operated in a data-dependent mode with the following parameters for the full-scan MS: resolution of 70,000 across 350-2000 *m/z*, AGC 3 x $10^6$, and maximum IT 50 ms. The full MS scan was followed by MS/MS for the top 10 precursor ions in each cycle with a NCE of 28 for unlabeled samples and 34 for TMT-labeled ones and dynamic exclusion of 30 s. Raw mass spectral data files (.raw) were searched using Proteome Discoverer (Thermo Fisher) and Mascot v2.4.1 (Matrix Science, Boston, MA). Mascot search parameters: 10 ppm mass tolerance for precursor ions; 10 mmu for fragment ion mass tolerance; 2 missed trypsin cleavages; fixed modifications: carbamidomethylation of cysteine and TMT 10plex modification of lysines and peptide N-termini; variable modifications:

oxidized methionine, ser phosphorylation, thr phosphorylation, and tyr phosphorylation. Only peptides with a Mascot score ≥25 and an isolation interference ≤30 were included in data analysis. TMT quantification was performed using Proteome Discoverer and isotopically-corrected per manufacturer's instructions, and the values were normalized to the median of each channel. Phosphopeptides were manually validated using CAMV software (*58*).

*Proteomics data analysis*

After pre-processing and summing signals from multiple spectra of the same peptide, TMT reporter ion signals of all unique TRM9L peptides were selected and, for each of the 10 channels, the geometric mean across all unique peptides was calculated to represent the relative abundance of TRM9L across all 10 channels. This was repeated for each unique TRM9L phosphopeptide. The abundance of each phosphopeptide was normalized by dividing each channel value by the abundance of the TRM9L protein in that channel. This ratio was reported as the "relative degree of phosphorylation" for each phosphopeptide in each channel. Data represent mean ± SD for three biological replicates. For comparing the degree of phosphorylation of a particular residue between two conditions, an unpaired Student T-test was performed ($p \leq 0.05$).

*TRM9L binding partners*

The coding region for TRM9L was cloned from cDNA isolated from 293T human embryonic kidney cells. The S214A, S255A, and S214A/S255A mutants of TRM9L were generated by Gibson Cloning. TRM9L constructs were cloned into a pcDNA3.1-FLAG-SBP expression vector or a pcDNA3.1-TWIN-STREP expression vector(*14*). Transient transfection and cellular extract production were performed as previously described(*14*). Whole-cell extract from transiently transfected cells cell lines (1 mg total protein) was rotated with 20 µL of Anti-DYKDDDDK Magnetic Beads (Takara BioUSA, Clontech) or Strep-Tactin XT-coated magnetic beads (# 2-

4090-002, IBA GmbH, Göttingen, Germany) for 2 hr at 4 °C in lysis buffer (20 mM HEPES, pH 7.9, 2 mM $MgCl_2$, 0.2 mM EGTA, 10% glycerol, 1 mM DTT, 0.1 mM PMSF, 0.1% NP-40, 150 mM NaCl). Resin was washed 3-times using the same buffer. Cellular extracts and purified protein samples were fractionated on NuPAGE Bis-Tris polyacrylamide gels (Thermo Fisher) followed by transfer to Immobilon FL PVDF membrane (EMD Millipore) for immunoblotting using antibodies noted earlier. Immunoblots were scanned using direct infrared fluorescence on the Odyssey System (LI-COR Biosciences). For silver staining compatible with mass spectrometry, gels were fixed for 1 hr at ambient temperature in 40% ethanol/10% acetic acid. Gels were sensitized using 30% ethanol/0.2% sodium thiosulphate/6.8% sodium acetate. Three 5-min washes with $H_2O$ followed. Gels were stained for 20 min with 0.25% silver nitrate followed by two 1-min washes with $H_2O$. The gel was developed with 2.5% sodium carbonate and 0.015% formaldehyde and stopped with 5% acetic acid. In-gel trypsin digestion and mass spectrometry was carried out at the University of Rochester Medical Center Mass Spectrometry Resource Laboratory. After the digestion, sample was desalted with a C18 column, and injected onto a Q Exactive Plus mass spectrometer operating in data-dependent mode. Raw data was searched against the SwissProt human database (www.uniprot.org), using MaxQuant (Max Planck Institute of Biochemistry, Martinsried, Germany) to identify proteins.

*Tumor formation assay*

Fertilized White Leghorn chicken eggs (Charles River Laboratories, MA) were incubated for 10 d at 37 °C in a humidified atmosphere inside a hatching incubator equipped with an automatic rotator (Octagon 20, Brinsea, Somerset, UK). On the day of the experiment, each eggshell was punctured in two locations: the long side of the egg and the side over the natural air sac. Using a suction device, an artificial air sac was created to separate the chorioallantoic membrane (CAM)

from the eggshell. A square window of ~1 cm was opened over the displaced CAM and sealed with a piece of sterile tape. SW620 cells expressing LacZ, WT TRM9L, and TRM9L mutants were detached from the plate with 2 mM EDTA in PBS and washed twice in PBS. Cells ($5x10^5$) were re-suspended in 50 µl PBS containing 1 mM $MgCl_2$, 0.5 mM $CaCl_2$, 100 U/ml penicillin and 100 µg/ml streptomycin and then inoculated into each CAM. The opening was re-sealed with tape and the eggs were placed in a stationary incubator at 37 °C for 7 d. The resulting tumors were excised and minced in a clean petri dish, then collagenased (type IA, Sigma-Aldrich) for 30 min at 37 °C. The number of tumor cells was counted with a hemocytometer. Each data point represents an independent biological sample, with error bars representing standard deviations and statistical significance determined using a Mann–Whitney test**.**

**Supplementary Materials**

• Supplementary Text

• Supplementary Figure S1. TRM9L transcript level predicts clinical prognosis.

• Supplementary Figure S2. TRM9L possesses a unique domain predicted to be intrinsically disordered and highly phosphorylated.

• Supplementary Figure S3. MS/MS spectra of phosphorylated tryptic peptides from TRM9L.

• Supplementary Figure S4. MS/MS spectra of phosphorylated tryptic peptides from TRM9L S380A mutant treated with H2O2.

•Supplementary Table S1: Kinase inhibitors screened for activity to block phosphorylation-dependent gel mobility shift of TRM9L.

**References and Notes**

1. L. X. Qin, Z. Y. Tang, J. S. Sham, Z. C. Ma, S. L. Ye, X. D. Zhou, Z. Q. Wu, J. M. Trent, X. Y. Guan, The association of chromosome 8p deletion and tumor metastasis in human hepatocellular carcinoma. *Cancer Res* **59**, 5662-5665 (1999).
2. C. E. Gustafson, P. J. Wilson, R. Lukeis, E. Baker, E. Woollatt, L. Annab, L. Hawke, J. C. Barrett, G. Chenevix-Trench, Functional evidence for a colorectal cancer tumor suppressor gene at chromosome 8p22-23 by monochromosome transfer. *Cancer Res* **56**, 5238-5245 (1996).
3. D. Birnbaum, J. Adelaide, C. Popovici, E. Charafe-Jauffret, M. J. Mozziconacci, M. Chaffanet, Chromosome arm 8p and cancer: a fragile hypothesis. *Lancet Oncol* **4**, 639-642 (2003).
4. J. C. Pole, C. Courtay-Cahen, M. J. Garcia, K. A. Blood, S. L. Cooke, A. E. Alsop, D. M. Tse, C. Caldas, P. A. Edwards, High-resolution analysis of chromosome rearrangements on 8p in breast, colon and pancreatic cancer reveals a complex pattern of loss, gain and translocation. *Oncogene* **25**, 5693-5706 (2006).
5. J. M. Flanagan, S. Healey, J. Young, V. Whitehall, D. A. Trott, R. F. Newbold, G. Chenevix-Trench, Mapping of a candidate colorectal cancer tumor-suppressor gene to a 900-kilobase region on the short arm of chromosome 8. *Genes Chromosomes Cancer* **40**, 247-260 (2004).
6. L. M. Voeghtly, K. Mamula, J. L. Campbell, C. D. Shriver, R. E. Ellsworth, Molecular alterations associated with breast cancer mortality. *PloS one* **7**, e46814 (2012).
7. J. Ashworth, B. Bernard, S. Reynolds, C. L. Plaisier, I. Shmulevich, N. S. Baliga, Structure-based predictions broadly link transcription factor mutations to gene expression changes in cancers. *Nucleic Acids Res* **42**, 12973-12983 (2014).
8. U. Begley, M. S. Sosa, A. Avivar-Valderas, A. Patil, L. Endres, Y. Estrada, C. T. Chan, D. Su, P. C. Dedon, J. A. Aguirre-Ghiso, T. Begley, A human tRNA methyltransferase 9-like protein prevents tumour growth by regulating LIN9 and HIF1-alpha. *EMBO Mol Med* **5**, 366-383 (2013).
9. B. Gyorffy, A. Lanczky, A. C. Eklund, C. Denkert, J. Budczies, Q. Li, Z. Szallasi, An online survival analysis tool to rapidly assess the effect of 22,277 genes on breast cancer prognosis using microarray data of 1,809 patients. *Breast Cancer Res Treat* **123**, 725-731 (2010).
10. B. Gyorffy, A. Lanczky, Z. Szallasi, Implementing an online tool for genome-wide validation of survival-associated biomarkers in ovarian-cancer using microarray data from 1287 patients. *Endocr Relat Cancer* **19**, 197-208 (2012).
11. S. L. Wang, J. A. Huang, X. Q. Liu, Mechanism of action of KIAA1456 gene on the proliferation and apoptosis of alveolar epithelial cells. *Eur Rev Med Pharmacol Sci* **21**, 600-605 (2017).
12. H. M. Chen, J. Wang, Y. F. Zhang, Y. H. Gao, Ovarian cancer proliferation and apoptosis are regulated by human transfer RNA methyltransferase 9-likevia LIN9. *Oncol Lett* **14**, 4461-4466 (2017).
13. H. R. Kalhor, S. Clarke, Novel methyltransferase for modified uridine residues at the wobble position of tRNA. *Mol Cell Biol* **23**, 9283-9292 (2003).
14. D. Fu, J. A. Brophy, C. T. Chan, K. A. Atmore, U. Begley, R. S. Paules, P. C. Dedon, T. J. Begley, L. D. Samson, Human AlkB homolog ABH8 Is a tRNA methyltransferase required for wobble uridine modification and DNA damage survival. *Mol Cell Biol* **30**, 2449-2459 (2010).

15. L. Songe-Moller, E. van den Born, V. Leihne, C. B. Vagbo, T. Kristoffersen, H. E. Krokan, F. Kirpekar, P. O. Falnes, A. Klungland, Mammalian ALKBH8 possesses tRNA methyltransferase activity required for the biogenesis of multiple wobble uridine modifications implicated in translational decoding. *Mol Cell Biol* **30**, 1814-1827 (2010).
16. J. Prilusky, C. E. Felder, T. Zeev-Ben-Mordehai, E. H. Rydberg, O. Man, J. S. Beckmann, I. Silman, J. L. Sussman, FoldIndex: a simple tool to predict whether a given protein sequence is intrinsically unfolded. *Bioinformatics* **21**, 3435-3438 (2005).
17. F. Gnad, J. Gunawardena, M. Mann, PHOSIDA 2011: the posttranslational modification database. *Nucleic Acids Res* **39**, D253-260 (2011).
18. A. Bah, R. M. Vernon, Z. Siddiqui, M. Krzeminski, R. Muhandiram, C. Zhao, N. Sonenberg, L. E. Kay, J. D. Forman-Kay, Folding of an intrinsically disordered protein by phosphorylation as a regulatory switch. *Nature* **519**, 106-109 (2015).
19. L. M. Iakoucheva, P. Radivojac, C. J. Brown, T. R. O'Connor, J. G. Sikes, Z. Obradovic, A. K. Dunker, The importance of intrinsic disorder for protein phosphorylation. *Nucleic Acids Res* **32**, 1037-1049 (2004).
20. O. Zugasti, W. Rul, P. Roux, C. Peyssonnaux, A. Eychene, T. F. Franke, P. Fort, U. Hibner, Raf-MEK-Erk cascade in anoikis is controlled by Rac1 and Cdc42 via Akt. *Mol Cell Biol* **21**, 6706-6717 (2001).
21. P. Lassus, P. Roux, O. Zugasti, A. Philips, P. Fort, U. Hibner, Extinction of rac1 and Cdc42Hs signalling defines a novel p53-dependent apoptotic pathway. *Oncogene* **19**, 2377-2385 (2000).
22. B. Zhao, L. Li, L. Wang, C. Y. Wang, J. Yu, K. L. Guan, Cell detachment activates the Hippo pathway via cytoskeleton reorganization to induce anoikis. *Genes Dev* **26**, 54-68 (2012).
23. M. A. Loza-Coll, S. Perera, W. Shi, J. Filmus, A transient increase in the activity of Src-family kinases induced by cell detachment delays anoikis of intestinal epithelial cells. *Oncogene* **24**, 1727-1737 (2005).
24. S. T. Eblen, J. K. Slack, M. J. Weber, A. D. Catling, Rac-PAK signaling stimulates extracellular signal-regulated kinase (ERK) activation by regulating formation of MEK1-ERK complexes. *Mol Cell Biol* **22**, 6023-6033 (2002).
25. K. Page, Y. Lange, Cell adhesion to fibronectin regulates membrane lipid biosynthesis through 5'-AMP-activated protein kinase. *J Biol Chem* **272**, 19339-19342 (1997).
26. N. Dephoure, K. L. Gould, S. P. Gygi, D. R. Kellogg, Mapping and analysis of phosphorylation sites: a quick guide for cell biologists. *Molecular biology of the cell* **24**, 535-542 (2013).
27. R. D. Guzy, B. Hoyos, E. Robin, H. Chen, L. Liu, K. D. Mansfield, M. C. Simon, U. Hammerling, P. T. Schumacker, Mitochondrial complex III is required for hypoxia-induced ROS production and cellular oxygen sensing. *Cell Metab* **1**, 401-408 (2005).
28. E. O. Hileman, J. Liu, M. Albitar, M. J. Keating, P. Huang, Intrinsic oxidative stress in cancer cells: a biochemical basis for therapeutic selectivity. *Cancer Chemother Pharmacol* **53**, 209-219 (2004).
29. M. B. Sporn, K. T. Liby, NRF2 and cancer: the good, the bad and the importance of context. *Nat Rev Cancer* **12**, 564-571 (2012).
30. E. Piskounova, M. Agathocleous, M. M. Murphy, Z. Hu, S. E. Huddlestun, Z. Zhao, A. M. Leitch, T. M. Johnson, R. J. DeBerardinis, S. J. Morrison, Oxidative stress inhibits distant metastasis by human melanoma cells. *Nature* **527**, 186-191 (2015).

31. B. Halliwell, J. M. C. Gutteridge, *Free radicals in biology and medicine*. (Oxford University Press, Oxford ; New York, ed. 4th, 2007), pp. xxxvi, 851 p., 858 p. of plates.
32. T. Finkel, Signal transduction by reactive oxygen species. *J Cell Biol* **194**, 7-15 (2011).
33. M. Schieber, N. S. Chandel, ROS function in redox signaling and oxidative stress. *Curr Biol* **24**, R453-462 (2014).
34. K. Z. Guyton, Y. Liu, M. Gorospe, Q. Xu, N. J. Holbrook, Activation of mitogen-activated protein kinase by H2O2. Role in cell survival following oxidant injury. *J Biol Chem* **271**, 4138-4142 (1996).
35. A. Meves, S. N. Stock, A. Beyerle, M. R. Pittelkow, D. Peus, H(2)O(2) mediates oxidative stress-induced epidermal growth factor receptor phosphorylation. *Toxicol Lett* **122**, 205-214 (2001).
36. I. Nakashima, K. Takeda, Y. Kawamoto, Y. Okuno, M. Kato, H. Suzuki, Redox control of catalytic activities of membrane-associated protein tyrosine kinases. *Archives of biochemistry and biophysics* **434**, 3-10 (2005).
37. A. Siebel, M. Cubillos-Rojas, R. C. Santos, T. Schneider, C. D. Bonan, R. Bartrons, F. Ventura, J. Rodrigues de Oliveira, J. L. Rosa, Contribution of S6K1/MAPK signaling pathways in the response to oxidative stress: activation of RSK and MSK by hydrogen peroxide. *PloS one* **8**, e75523 (2013).
38. C. M. Rosseland, L. Wierod, M. P. Oksvold, H. Werner, A. C. Ostvold, G. H. Thoresen, R. E. Paulsen, H. S. Huitfeldt, E. Skarpen, Cytoplasmic retention of peroxide-activated ERK provides survival in primary cultures of rat hepatocytes. *Hepatology* **42**, 200-207 (2005).
39. R. Lara, M. J. Seckl, O. E. Pardo, The p90 RSK family members: common functions and isoform specificity. *Cancer Res* **73**, 5301-5308 (2013).
40. V. Oza, S. Ashwell, L. Almeida, P. Brassil, J. Breed, C. Deng, T. Gero, M. Grondine, C. Horn, S. Ioannidis, D. Liu, P. Lyne, N. Newcombe, M. Pass, J. Read, S. Ready, S. Rowsell, M. Su, D. Toader, M. Vasbinder, D. Yu, Y. Yu, Y. Xue, S. Zabludoff, J. Janetka, Discovery of checkpoint kinase inhibitor (S)-5-(3-fluorophenyl)-N-(piperidin-3-yl)-3-ureidothiophene-2-carboxamide (AZD7762) by structure-based design and optimization of thiophenecarboxamide ureas. *J Med Chem* **55**, 5130-5142 (2012).
41. M. Saha, A. Carriere, M. Cheerathodi, X. Zhang, G. Lavoie, J. Rush, P. P. Roux, B. A. Ballif, RSK phosphorylates SOS1 creating 14-3-3-docking sites and negatively regulating MAPK activation. *Biochem J* **447**, 159-166 (2012).
42. J. A. Galan, K. M. Geraghty, G. Lavoie, E. Kanshin, J. Tcherkezian, V. Calabrese, G. R. Jeschke, B. E. Turk, B. A. Ballif, J. Blenis, P. Thibault, P. P. Roux, Phosphoproteomic analysis identifies the tumor suppressor PDCD4 as a RSK substrate negatively regulated by 14-3-3. *Proc Natl Acad Sci U S A* **111**, E2918-2927 (2014).
43. S. Chen, S. Synowsky, M. Tinti, C. MacKintosh, The capture of phosphoproteins by 14-3-3 proteins mediates actions of insulin. *Trends Endocrinol Metab* **22**, 429-436 (2011).
44. E. Wilker, M. B. Yaffe, 14-3-3 Proteins--a focus on cancer and human disease. *Journal of molecular and cellular cardiology* **37**, 633-642 (2004).
45. A. K. Gardino, M. B. Yaffe, 14-3-3 proteins as signaling integration points for cell cycle control and apoptosis. *Seminars in cell & developmental biology* **22**, 688-695 (2011).
46. R. Anjum, J. Blenis, The RSK family of kinases: emerging roles in cellular signalling. *Nat Rev Mol Cell Biol* **9**, 747-758 (2008).

47. P. Nowak-Sliwinska, T. Segura, M. L. Iruela-Arispe, The chicken chorioallantoic membrane model in biology, medicine and bioengineering. *Angiogenesis* **17**, 779-804 (2014).
48. E. I. Deryugina, J. P. Quigley, Chick embryo chorioallantoic membrane model systems to study and visualize human tumor cell metastasis. *Histochem Cell Biol* **130**, 1119-1130 (2008).
49. P. J. Roberts, C. J. Der, Targeting the Raf-MEK-ERK mitogen-activated protein kinase cascade for the treatment of cancer. *Oncogene* **26**, 3291-3310 (2007).
50. P. C. Dedon, S. R. Tannenbaum, Reactive nitrogen species in the chemical biology of inflammation. *Archives of biochemistry and biophysics* **423**, 12-22 (2004).
51. W. C. Lee, C. H. Choi, S. H. Cha, H. L. Oh, Y. K. Kim, Role of ERK in hydrogen peroxide-induced cell death of human glioma cells. *Neurochem Res* **30**, 263-270 (2005).
52. P. O'Neill, in *Radiation chemistry: present status and future trends,* C. D. Jonah, B. S. M. Rao, Eds. (Elsevier Science, 2001), vol. 87, pp. 585-622.
53. E. I. Azzam, J. P. Jay-Gerin, D. Pain, Ionizing radiation-induced metabolic oxidative stress and prolonged cell injury. *Cancer Letters* **327**, 48-60 (2012).
54. S. Desaint, S. Luriau, J. C. Aude, G. Rousselet, M. B. Toledano, Mammalian Antioxidant Defenses Are Not Inducible by H2O2. *J Biol Chem* **279**, 31157–31163 (2004).
55. V. Goss Tusher, R. Tibshirani, G. Chu, Significance analysis of microarrays applied to the ionizing radiation response. *Proceedings of the National Academy of Science USA* **98**, 5116–5121 (2001).
56. S. Stöcker, K. Van Laer, A. Mijuskovic, T. P. Dick, The Conundrum of Hydrogen Peroxide Signaling and the Emerging Role of Peroxiredoxins as Redox Relay Hubs. *Antioxid Redox Signal*, (2017).
57. S. B. Ficarro, G. Adelmant, M. N. Tomar, Y. Zhang, V. J. Cheng, J. A. Marto, Magnetic bead processor for rapid evaluation and optimization of parameters for phosphopeptide enrichment. *Anal Chem* **81**, 4566-4575 (2009).
58. T. G. Curran, B. D. Bryson, M. Reigelhaupt, H. Johnson, F. M. White, Computer aided manual validation of mass spectrometry-based proteomic data. *Methods* **61**, 219-226 (2013).

**Acknowledgments:** The authors thank Dr. Amanda Del Rosario and Richard Schiavoni for assistance with phosphoproteomics at the Proteomics Core of MIT Koch Institute Swanson Biotechnology Center, and Yan Li for assistance with the cloning of TRM9L mutants. **Funding**: CG was supported by a David H. Koch Cancer Fellowship, a Howard Hughes Medical Institute International Student Research Fellowship, and a Siebel Scholarship. DF was supported by the National Science Foundation CAREER Award 1552126. TB and PD were supported by grants ES026856 and ES024615 from the National Institute of Environmental Health Sciences. **Author**

**contributions**: CG participated in study design, performing the bulk of the experiments, interpreting data and manuscript writing. JR designed and executed the 14-3-3 studies, interpreting data and manuscript writing. UB constructed TRM9L cell lines, performed xenograft studies, and contributed to study design and manuscript writing. DF, TB and PD contributed to study design, data interpretation, and manuscript writing. **Competing interests**: The authors declare that they have no conflicts of interest with the contents of this article. The content is solely the responsibility of the authors and does not necessarily represent the official views of the National Institutes of Health. **Data and materials availability**: Mass spectrometry data were deposited in Chorus (https://www.chorusproject.org) Project ID 1336: Experiment *Phosphorylation sites of TRM9L in HCT116 cells.* Experiment *Phosphorylation of TRM9L WT and S380A mutant under H2O2 treatment.* Experiment *Dynamics of TRM9L phosphorylation under H2O2 treatment.* Experiment *Binding partners of ALKBH8 and TRM9L in HEK293 cells.*

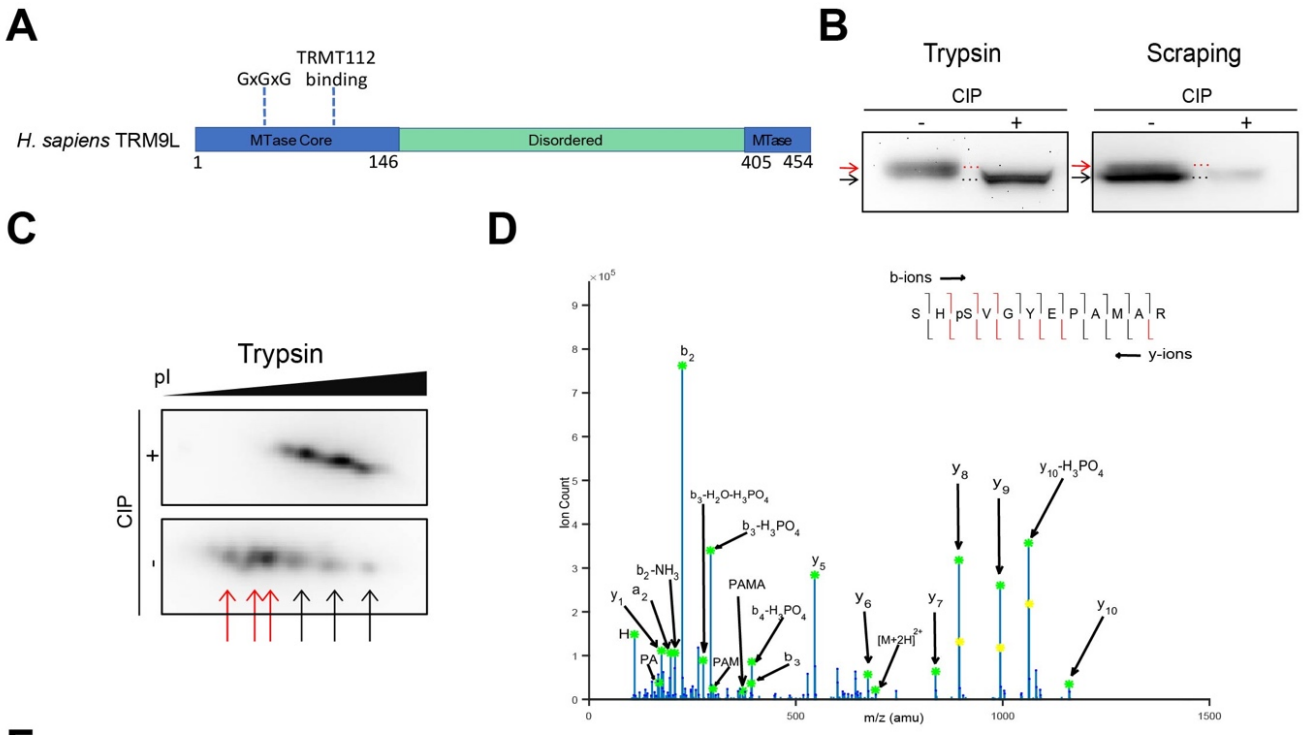


E

```
147...KNRHFEKQDVLVPWNRALCSQLFSESSQSGRKRQCGYPERGHPYHPPCSECSCSVCFKEQC
     14-3-3 binding motif
208  GSKRSHSVGYEPAMARTCFANISKEGEEEYGFYSTLGKSFRSWFFSRSLDESTLRKQIERV

269  RPLKNTEVWASSTVTVQPSRHSSLDFDHQEPFSTKGQSLDEEVFVESSSGKHLEWLRAPGT
                                                  RSK motif
330  LKHLNGDHQGEMRRNGGGNFLDSTNTGVNCVDAGNIEDDNPSASKILRRISAVDSTDFNPD

391  DTMSVEDPQTDVLD...
```

**Fig. 1**. Phosphorylation of the TRM9L disordered domain. **A.** Schematic of human TRM9L with conserved N- and C-terminal methyltransferase domains labeled in blue, the non-homologous internal domain in green. **B.** Immunoblot analysis of total lysate of HCT116 cell expressing FLAG-TRM9L treated without or with calf intestinal phosphatase (CIP). **C.** Two-dimensional SDS-PAGE immunoblot analysis of HCT116 cell lysates showing multiple phosphorylation states. **D.** Representative MS/MS spectrum of the tryptic TRM9L peptide spanning phosphorylated $Ser^{214}$ (SHpSVGYEPAMAR). **E.** Primary sequence of the non-homologous internal domain of TRM9L with phosphorylated residues labeled in red.

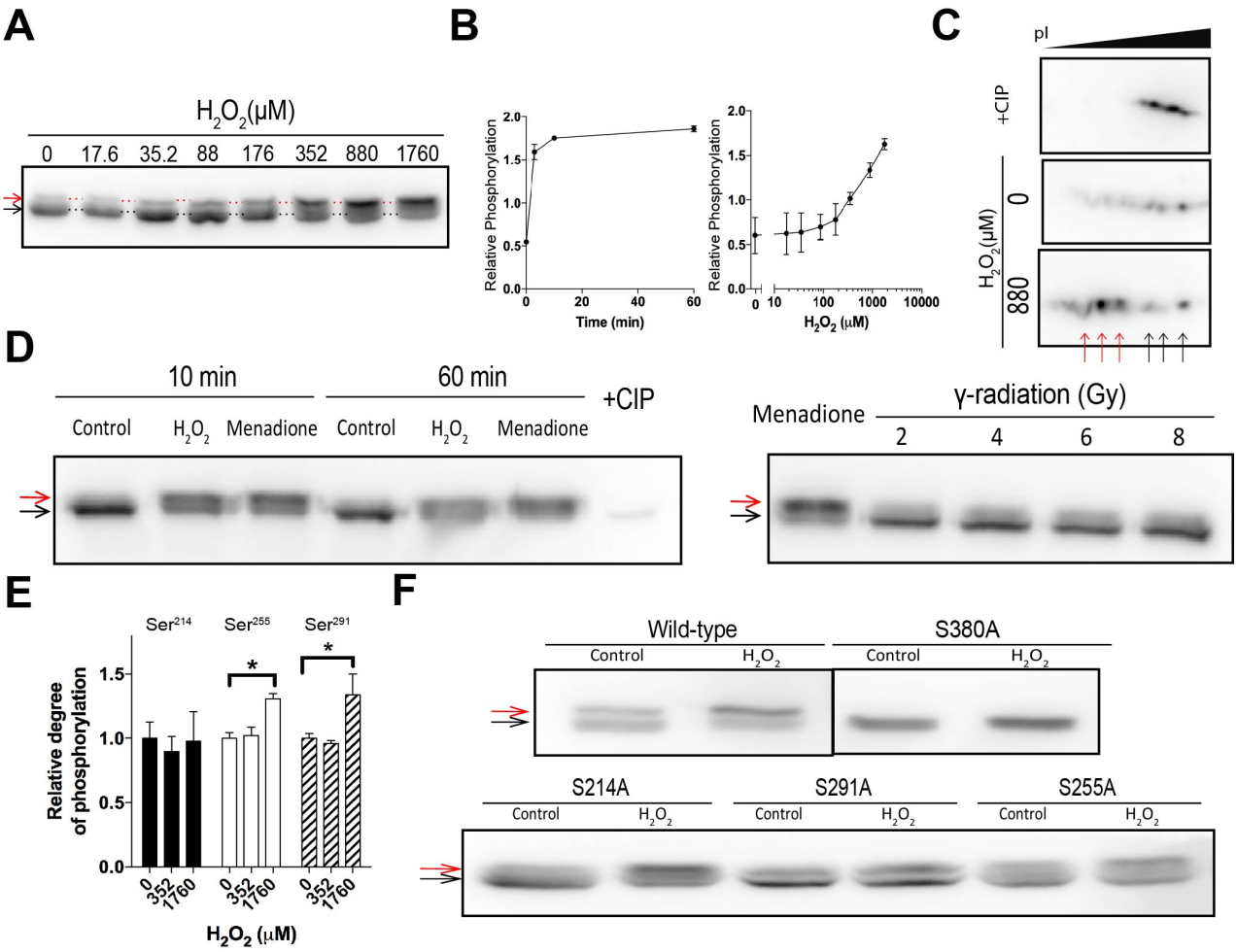


**Fig. 2.** Hyperphosphorylation of TRM9L induced by oxidative stress. **A.** Treatment with $H_2O_2$ induce TRM9L hyperphosphorylation. **B.** *Left:* Kinetics of TRM9L hyperphosphorylation by exposure to 880 μM $H_2O_2$. *Right:* $H_2O_2$ dose-response for TRM9L hyperphosphorylation 10 min after exposure; data represent mean ± SD (N=3); data represent mean ± SD (N=3). **C.** 2D gel analysis reveals multiple sites of $H_2O_2$-induced TRM9L phosphorylation. **D.** Menadione induces TRM9L phosphorylation while γ-radiation of HCT116 cells has no major effect on TRM9L phosphorylation status. **E.** Quantitative phosphoproteomics reveals $H_2O_2$-induced increases in phosphorylation at $Ser^{255}$ (white) and $Ser^{291}$ (shaded) but not $Ser^{214}$ (black); data represent mean ± SD (N = 3 at each dose of $H_2O_2$). **F.** $H_2O_2$-induced $Ser^{380}$ phosphorylation, but not other sites, determines the 1D gel mobility shift.

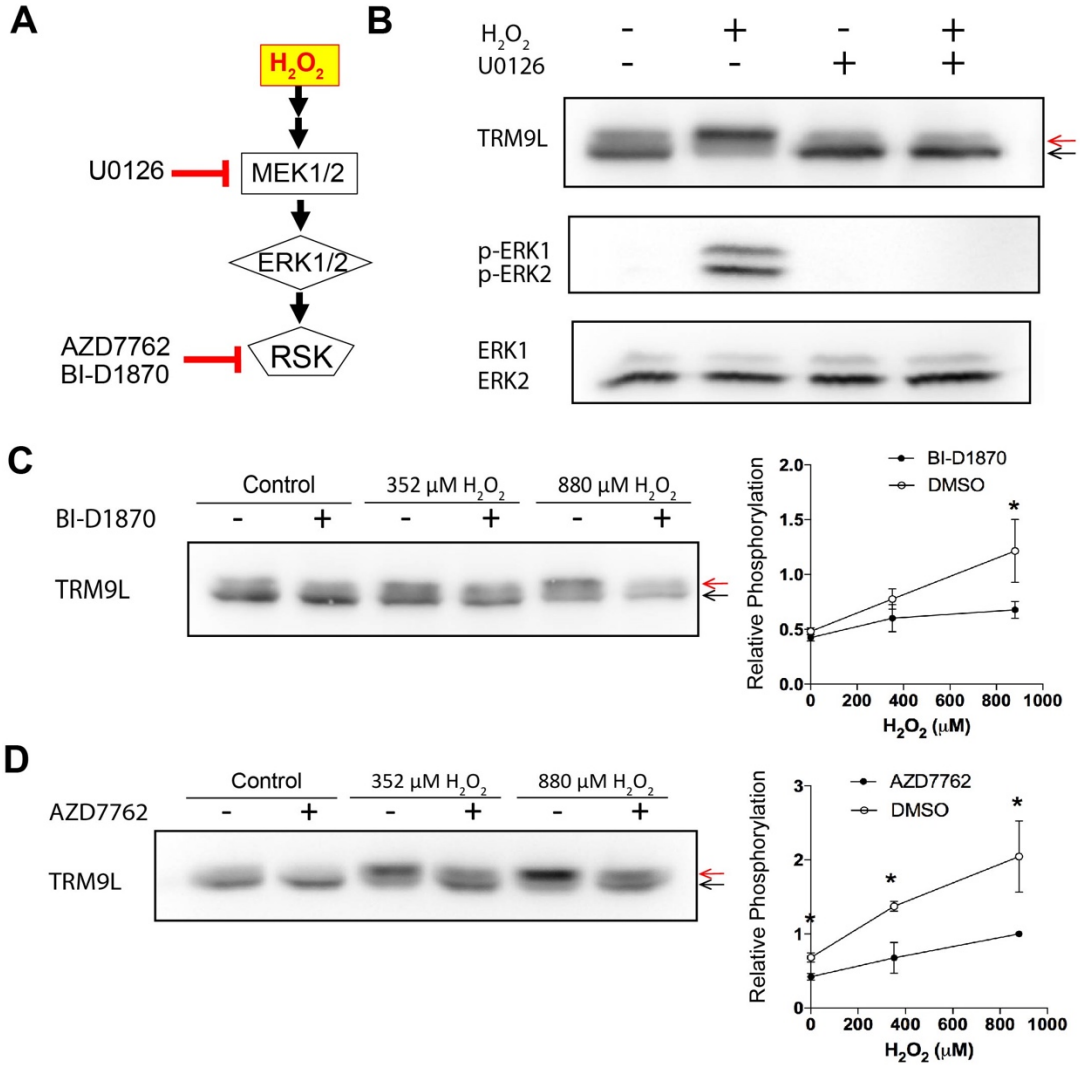


**Fig. 3.** $H_2O_2$-induced hyperphosphorylation of TRM9L is dependent upon the ERK- and RSK-signaling pathways. **A.** Simplified schematic of the MEK/ERK signaling pathways transduced through RSK. **B.** $H_2O_2$-induced autophosphorylation of ERK1/2 and hyperphosphorylation of TRM9L are abolished using ERK1/2 inhibitor U0126. **C&D.** *Left:* $H_2O_2$-induced hyperphosphorylation of TRM9L is inhibited by the RSK inhibitors AZD7762 and BI-D1870. *Right:* Quantification of $H_2O_2$-induced hyperphosphorylation of $Ser^{380}$ in the presence of DMSO or RSK inhibitor. Data represent mean ± SD (N=3).

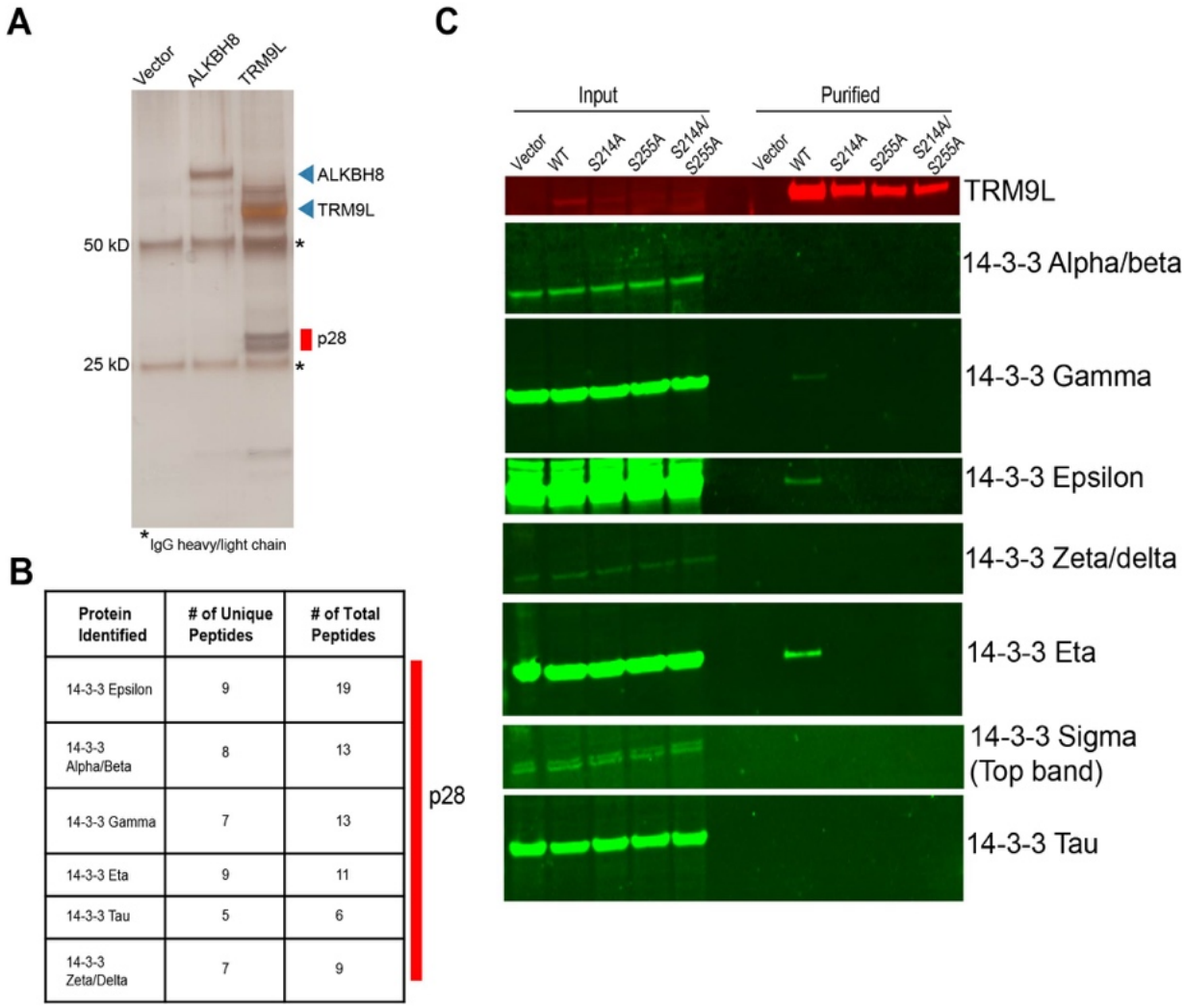


| Protein Identified | # of Unique Peptides | # of Total Peptides |
|---|---|---|
| 14-3-3 Epsilon | 9 | 19 |
| 14-3-3 Alpha/Beta | 8 | 13 |
| 14-3-3 Gamma | 7 | 13 |
| 14-3-3 Eta | 9 | 11 |
| 14-3-3 Tau | 5 | 6 |
| 14-3-3 Zeta/Delta | 7 | 9 |

p28

**Fig. 4.** Phosphorylation-dependent interaction of TRM9L with 14-3-3 proteins. **A.** Immunoprecipitation of TRM9L, but not ALKBH8, carried 28 kD proteins (p28). **B.** Mass spectrometric analysis of proteins co-precipitating with TRM9L reveals 14-3-3 isoforms. **C.** Immunoblot identification of 14-3-3 gamma, eta, and epsilon bound to TRM9L in a pS214- and pS255-dependent manner and loss of phosphorylation in the S214A and S255A mutants abolished the 14-3-3 interaction.

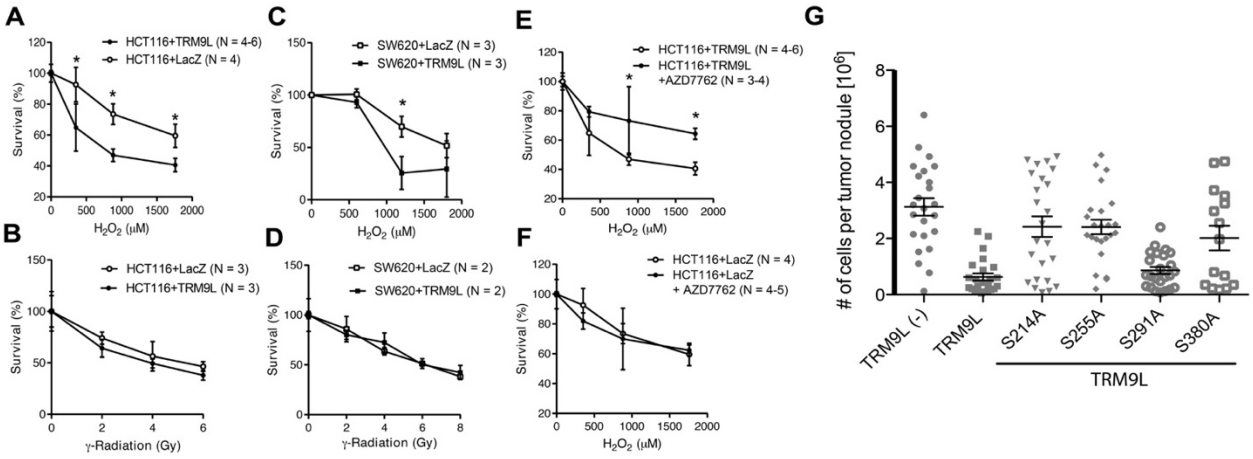


**Fig. 5.** Multiple TRM9L phosphorylation sites link ROS signaling and tumor growth suppression. **A-F.** Survival of cells 24 hrs after $H_2O_2$ treatment or ionizing radiation. data represent mean $\pm$ SD and asterisks denote significance ($p \leqslant 0.05$) in a Student T-test. **G.** Relative to WT TRM9L-expressing cells, tumor growth (CAM xenografts) is suppressed by phosphorylation at $Ser^{214}$ ($p< 0.0007$), $Ser^{255}$ ($p<0.0001$), and $Ser^{380}$ ($p<0.01$). Bars represent mean ± SD for the data representing individual tumor samples, with a Mann-Whitney test for significance.

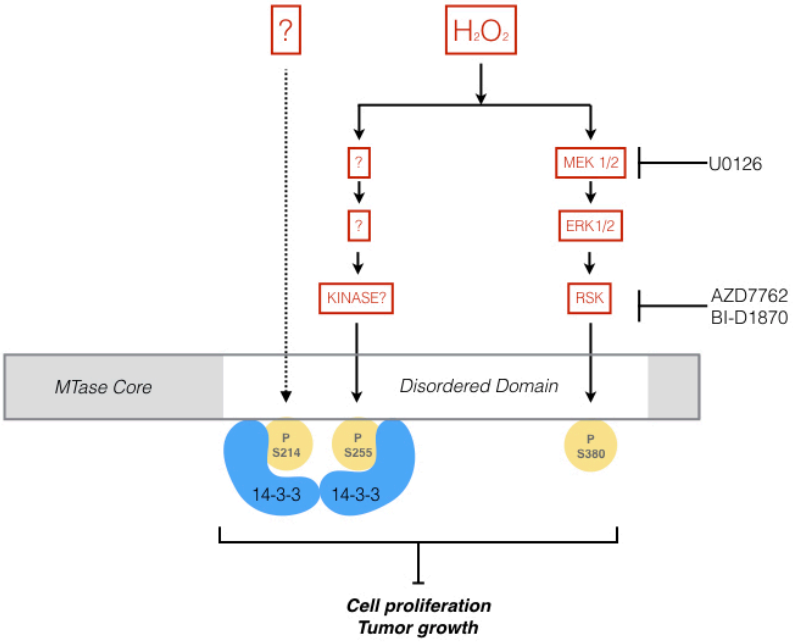


**Fig. 6.** Phosphorylation of human TRM9L is a critical regulator of oxidative stress survival and tumor growth suppression.

**Supplementary Materials**

• Supplementary Text

• Supplementary Figure S1. TRM9L transcript level predicts clinical prognosis.

• Supplementary Figure S2. TRM9L possesses a unique domain predicted to be intrinsically disordered and highly phosphorylated.

• Supplementary Figure S3. MS/MS spectra of phosphorylated tryptic peptides from TRM9L (WT).

• Supplementary Figure S4. MS/MS spectra of phosphorylated tryptic peptides from TRM9L S380A mutant treated with H2O2.

•Supplementary Table S1: Kinase inhibitors screened for activity to block phosphorylation-dependent gel mobility shift of TRM9L.

**Supplementary Text**

**Methods and Materials**

***Construction of plasmids for stable expression of TRM9L mutants***. pBABE-puro-TRM9L-3xFLAG was used as a template for following PCR reactions. The TRM9L ORF originated from Origene plasmid RC203720. The backbone vector pBABE-puro was purchased from Addgene, Cambridge, MA. A sequence from the multiple cloning site of the pCMV-3Tag-3A plasmid (Agilent Technologies #240197, Santa Clara, CA) containing a 3xFLAG tag sequence was inserted between the EcoRI and the SalI sites of the backbone to create a new vector pBABE-puro-3xFLAG. TRM9L ORF was cloned into the final destination vector pBABE-puro-3xFLAG between EcoRI and XhoI sites. 3xFLAG was located at the C-terminus of TRM9L. For the TRM9L S214A mutant, S214A reverse primer was used with pBABE 5' forward primer to PCR amplify a MEGAPRIMER containing the S214A mutation. PCR-purified S214A MEGAPRIMER was used in a second PCR reaction with pBABE 3' reverse primer to amplify the entire KIAA1456 ORF containing the mutation and the restriction sites EcoRI and XhoI at the ends to clone it back into the destination vector pBABE-puro-3xFLAG. For the S255A and S291A mutants, S255A and S291A forward primers were used, respectively, with pBABE 3' reverse primer to PCR amplify MEGAPRIMERS that contain each mutation. PCR-purified MEGAPRIMERS were then used in a second PCR reaction with pBABE 5' forward primer to amplify the entire KIAA1456 ORF containing each mutation and the restriction sites EcoRI and XhoI at the ends to clone it back into the destination vector pBABE-puro-3xFLAG.

S214A reverse primer: 5' ttcatagcccacGGCgtgggaccgtttt 3'

S255A forward primer: 5' gtttttctccagaGCTttggatgaatcgact 3'

S291A forward primer: 5' ttccagacactctGCTctagactttgatca 3'

pBABE 3' reverse primer: 5' ACCCTAACTGACACACATTCC 3'

pBABE 5' forward primer: 5' CTTTATCCAGCCCTCAC 3'

For the TRM9L S380A mutant, mutation serine (TGT) to alanine (GCA) at position 380 of the commercial pCMV-TRM9L vector (Origene RC203720, Rockville, MD) was achieved using the Q5 site-directed mutagenesis kit (NEB #E0554S). Primers used for mutagenesis: 5'-GAGAAGGATTgcaGCAGTCGATTC; 5'-AATATTTTACTAGCAGAAGGATTATC. The TRM9L S380A mutant ORF was then cloned into the destination vector pBABE-puro-3xFLAG between EcoRI and XhoI sites. The TRM9L S380A mutant protein was also expressed in HCT116 cells via transient transfection of the Origene pCMV-TRM9L (S380A) plasmid using the standard Invitrogen Lipofectamine 2000 protocol (Thermo Fisher Scientific).

***Treatment with kinase inhibitors***. Cells ($1 \times 10^6$) were seeded into wells of a 6-well plate and covered with 2 ml of media. After overnight incubation, the following kinase inhibitors were diluted in DMSO and added at noted final concentrations: SB203580 (10 μM), P38 α/β inhibitor (Santa Cruz Biotechnology sc-3533); SB202190 (5 μM), P38 α/β inhibitor (Sigma-Aldrich S7067); Doramapimod (1 μM), potent inhibitor against all 4 P38 isoforms (Cayman Chemicals # 10460); SP600125 (25 μM), JNK inhibitor (Cayman Chemicals # 10010466); NQDI-1 (25 μM), ASK1 inhibitor (Sigma-Aldrich SML0185); KU55933 (10 μM), ATM inhibitor (Sigma-Aldrich SML1109); VE821 (10 μM), ATR inhibitor (Cayman Chemicals # 17587); SCH900776 (1 μM), selective inhibitor against checkpoint kinase 1 (CHEK1) (Cayman Chemicals # 18131); Chk2 inhibitor II (5 μM), selective inhibitor against checkpoint kinase 2 (CHEK2) (Cayman Chemicals # 17552); KN62 (10 μM), CAMK2 inhibitor (Cayman Chemicals # 13318); D4476 (10 μM), CK1 inhibitor (Cayman Chemicals # 13305); TBCA (25 μM), CK2 inhibitor (Sigma-Aldrich SML0854); lithium chloride (LiCl dissolved in PBS, 10 mM), GSK3β inhibitor (Sigma-Aldrich); SB216763 (10 μM), selective GSK3β inhibitor (Cayman Chemicals # 10010246); CRT0066101 (71 nM), PKD inhibitor (Cayman Chemicals # 15337); IPA-3 (20 μM), PAK1 inhibitor (Cayman chemicals # 14759); PD98059 (50 μM), selective MEK1 inhibitor that also moderately inhibits MEK2 (Cayman Chemicals # 10006726). Cells were further incubated at 37 °C for additional 90 min and then treated with oxidants as described in the main text. Kinase inhibitors were also added to the desired concentration into the FBS-free media used for $H_2O_2$ treatment.

**Supplementary Figures and Tables**

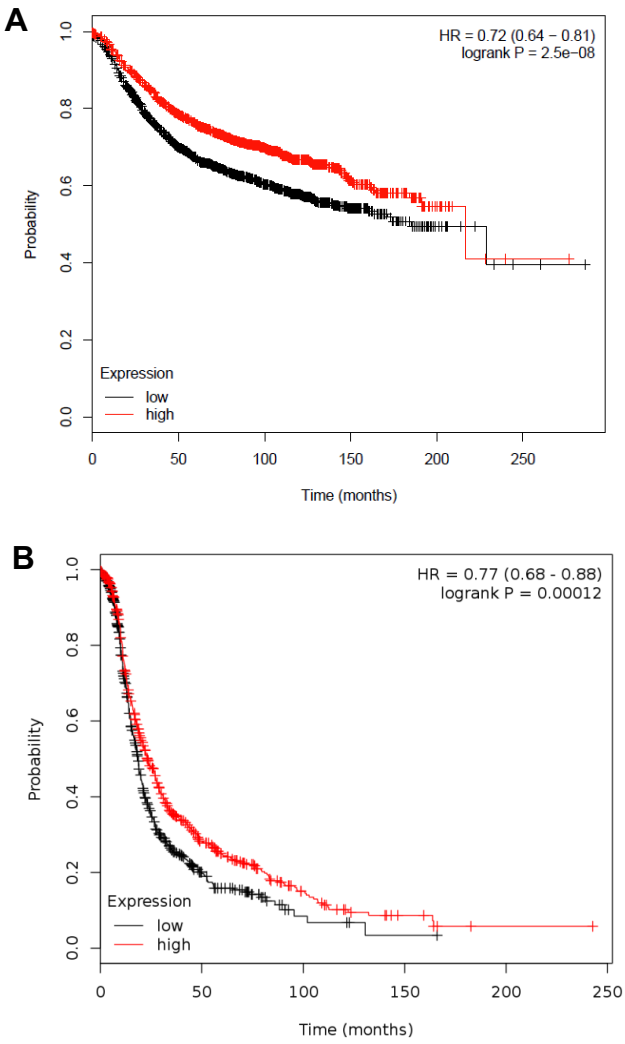


**Supplementary Figure S1. TRM9L transcript level predicts clinical prognosis**. **A.** Low TRM9L expression level is significantly associated with short relapse-free survival of breast cancer. **B.** Low TRM9L expression level is significantly associated with short progression-free survival of ovarian cancer. The Kaplan-Meier survival curves were generated by kmplot.com. For each cancer type, the survival of patients with lower 50% KIAA1456 (TRM9L) expression level was plotted in black; that with higher 50% expression level was in red. HR stands for hazard ratio. Statistical significance was determined by the Cox proportional hazards regression method.

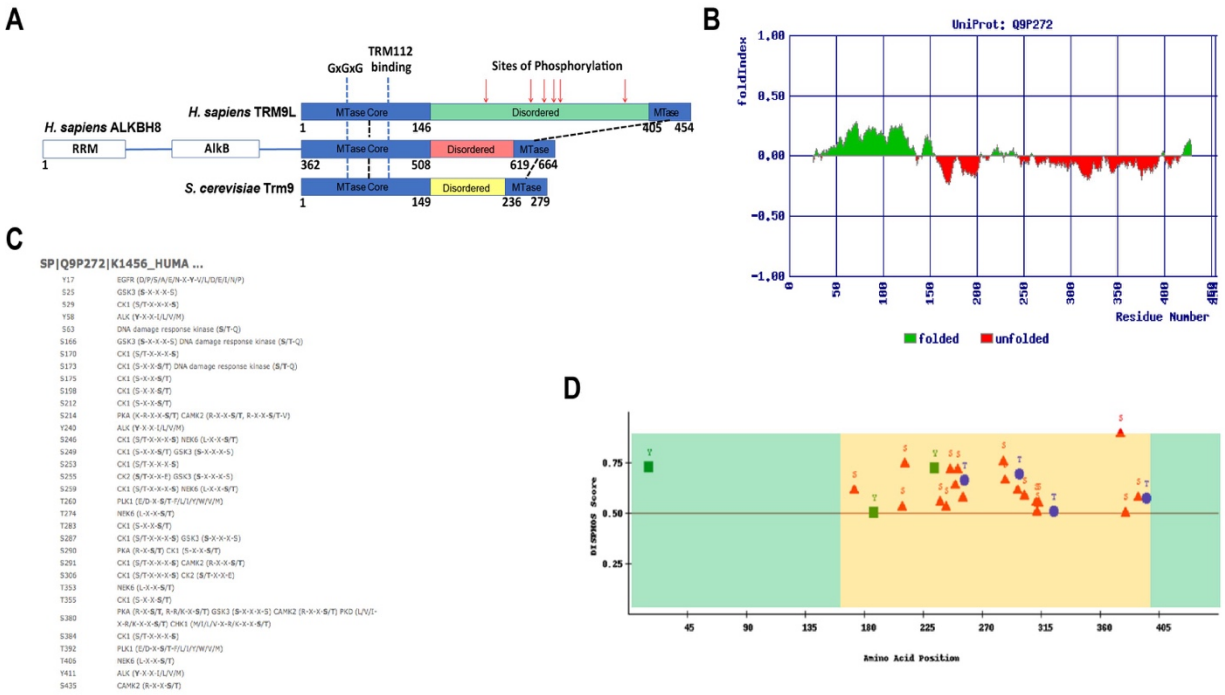


**Supplementary Figure S2. TRM9L possesses a unique domain predicted to be intrinsically disordered and highly phosphorylated**. **A.** Comparison of the primary sequence of human TRM9L, human ALKBH8, and yeast Trm9. The conserved methyltransferase domain is labeled in blue. **B.** The internal domain of TRM9L is predicted to be intrinsically disordered by FoldIndex. Green stands for the regions predicted to be folded and red for those predicted to be unfolded. **C.** Kinase phosphorylation motifs on TRM9L as predicted by PHOSIDA. **D.** The internal domain of TRM9L is predicted to be highly phosphorylated by DISPHOS. S/T/Y residues predicted to be phosphorylated are marked. Green represents the N-terminal and C-terminal regions labeled as folded in panel **B** and yellow the internal domain labeled as unfolded in panel **B**.

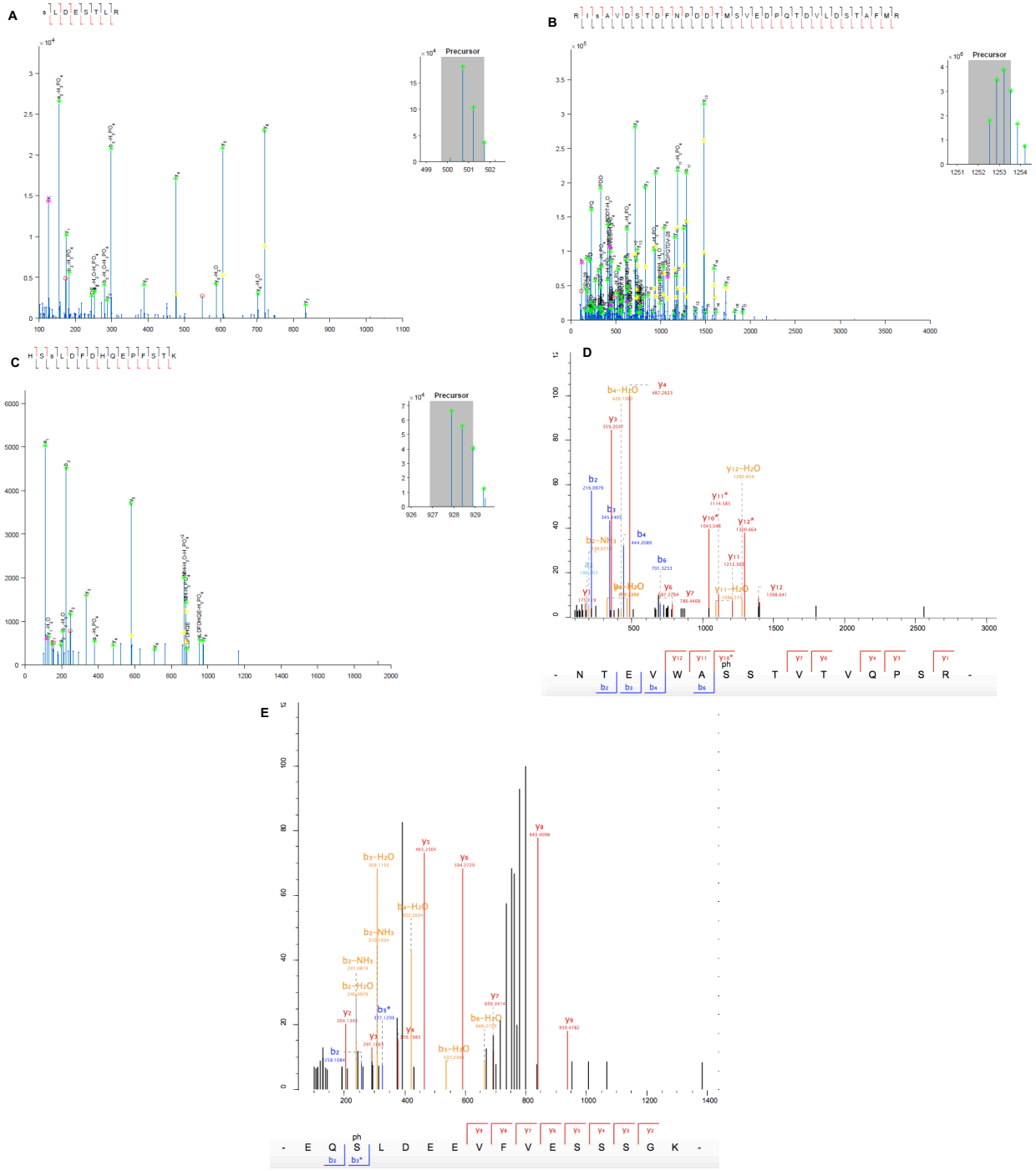


**Supplementary Figure S3. MS/MS spectra of phosphorylated tryptic peptides from TRM9L**. **A.** CID of pS255-containing peptide. **B.** CID of pS380-containing peptide. **C.** CID of pS291-containing peptide. **D.** CID of pS279-containing peptide. **E**. CID of pS306-containing peptide. Panel **A**, **B**, and **C** were generated with Mascot and CAMV. Green star represents an annotated b- or y-ion; yellow represents an isotope peak; red circle indicates an unannotated peak; magenta star represents an internal fragment. Panel **D** and **E** were generated using MaxQuant. Annotated b-ion peaks were labeled in blue and yellow; annotated y-ion peaks in red.

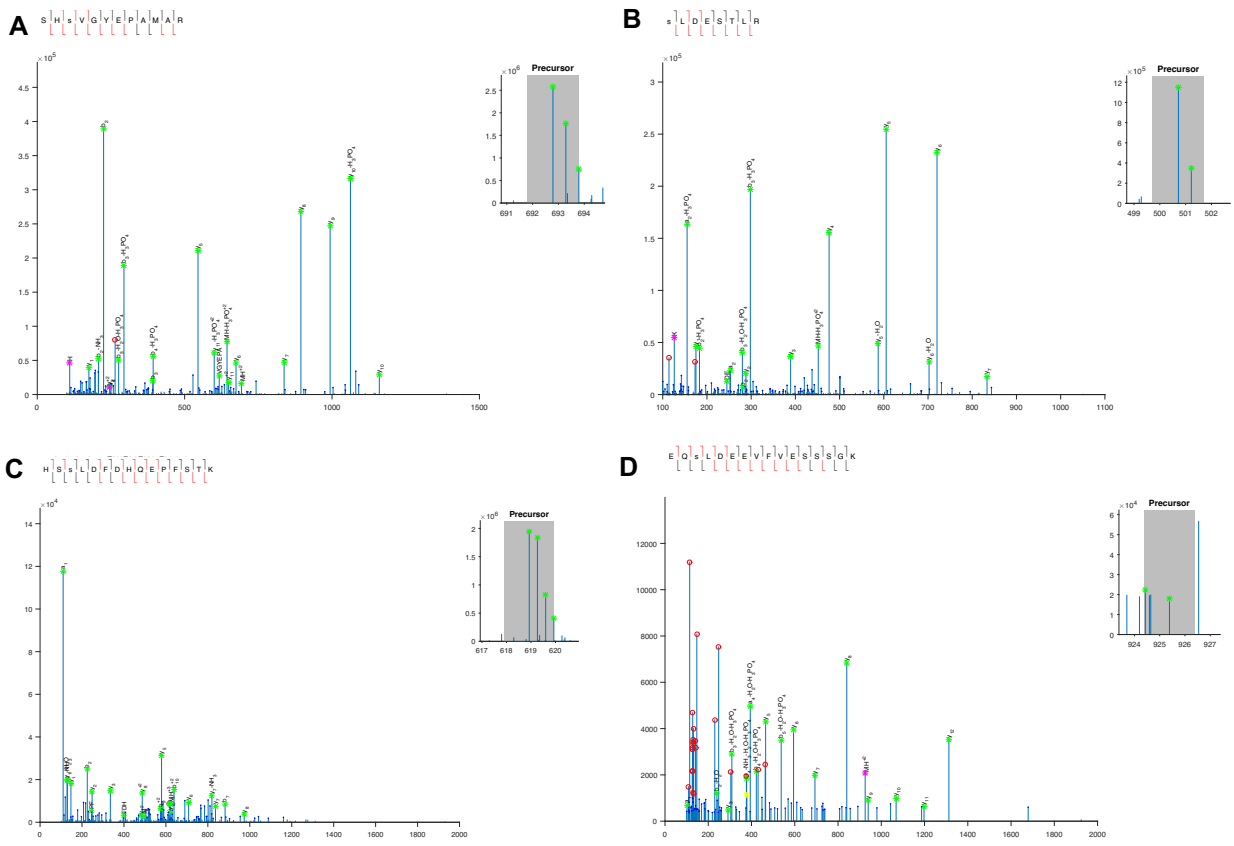


**Supplementary Figure S4. MS/MS spectra of phosphorylated tryptic peptides from TRM9L S380A mutant treated with $H_2O_2$.** **A.** CID of pS214-containing peptide. **B.** CID of pS255-containing peptide. **C.** CID of pS291-containing peptide. **D.** CID of pS306-containing peptide. Panels were generated with Mascot and CAMV. Green star represents an annotated b- or y-ion; yellow represents an isotope peak; red circle indicates an unannotated peak; magenta star represents an internal fragment. HCT116+LacZ cells transiently transfected with a TRM9L(S380A)-expressing plasmid were treated with 880 µM H2O2 for 15 min before the analysis by phosphoproteomics.

| Kinase | Inhibitor | Inhibition of TRM9L hyperphosphorylation |
|---|---|---|
| P38 (α/β) | SB202190 | N |
| P38 (α/β) | SB203580 | N |
| P38 (all isoforms) | Doramapimod | N |
| ASK1 | NQDI-1 | N |
| JNK | SP600125 | N |
| ATM | KU55933 | N |
| ATR | VE821 | N |
| CHEK1 | SCH900776 | N |
| CHEK2 | Chk2 Inhibitor II | N* |
| CAMK2 | KN62 | N |
| GSK3β | LiCl | N |
| GSK3β | SB216763 | N |
| PKD | CRT0066101 | N |
| CK1 | D4476 | N |
| CK2 | TBCA | N |
| PAK1 | IPA-3 | N |
| RSK2/3 | AZD7762 | Y |
| RSK (all isoforms) | BI-D1870 | Y |
| MEK1/2 | U0126 | Y |
| MEK1/2 | PD98059 | Y |

**Supplementary Table S1.** Kinase inhibitors screened for activity to block phosphorylation- dependent gel mobility shift of TRM9L. *Chk2 Inhibitor II at the dose tested promotes the 1D gel mobility shift of TRM9L in untreated cells but inhibits the H2O2-induced mobility shift.